Ultramicroscopy 111 (2011) 1720–1733

Contents lists available at SciVerse ScienceDirect

Ultramicroscopy

journal homepage: www.elsevier.com/locate/ultramic

Grain detection from 2d and 3d EBSD data—Specification of the MTEX algorithm

Florian Bachmann [a], Ralf Hielscher [b,*], Helmut Schaeben [a]

[a] Geoscience Mathematics and Informatics, TU Bergakademie Freiberg, Germany
[b] Applied Functional Analysis, TU Chemnitz, Germany

ARTICLE INFO

Article history:
Received 12 April 2011
Received in revised form
1 August 2011
Accepted 9 August 2011
Available online 7 September 2011

Keywords:
EBSD data
Grain detection
Grain boundary reconstruction
Crystallographic preferred orientation
Individual orientation measurements
Texture analysis
Fabric analysis
Software toolbox MTEX

ABSTRACT

We present a fast and versatile algorithm for the reconstruction of the grain structure from 2d and 3d Electron Back Scatter Diffraction (EBSD) data. The algorithm is rigorously derived from the modeling assumption that grain boundaries are located at the bisectors of adjacent measurement locations. This modeling assumption immediately implies that grains are composed of Voronoi cells corresponding to the measurement locations. Thus our algorithm is based on the Voronoi decomposition of the 2d or 3d measurement domain. It applies to any geometrical configuration of measurement locations and allows for missing data due to measurement errors. The definition of grains as compositions of Voronoi cells implies another fundamental feature of the proposed algorithm—its invariance with respect to spatial displacements, i.e., rotations or shifts of the specimen. This paper also serves as a reference paper for the texture analysis software MTEX, which is a comprehensive and versatile, freely available MATLAB toolbox that covers a wide range of problems in quantitative texture analysis, including the analysis of EBSD data.

1. Introduction and motivation

Ever since its automation [1,2] EBSD has become an increasingly widespread and major technique to analyze texture, fabric, and anisotropic properties of polycrysatlline materials; for a comprehensive survey of applications the reader is referred to Rollett et al. [3].

In our communication we consider EBSD data, i.e., spatially referenced measurements of individual crystallographic orientations, and elaborate on a mathematically sound method to recover the underlaying microstructure, i.e., the grains and grain boundaries. We shall explicitly state its modeling assumptions and present a corresponding algorithm that works for conventional 2d data as well as for 3d data as they can be measured by recent EBSD systems.

We consider the data as a list of triples (x_ℓ, o_ℓ, p_ℓ), $\ell = 1,\dots,L$, where $x_\ell \in D \subset \mathbb{R}^3$ denotes the location of the measurement, $p_\ell \in \{1,\dots,N_p\}$ is the phase information, and $o_\ell \in \mathrm{SO}(3)$ denotes the orientation. Note that we do not assume any regular arrangement of the measurement locations. Data sampled with EBSD systems are commonly located on an initially regular hexagonal or square grid. However, removing or neglecting some of the data due to poor indexing generally results in an irregular grid. Formulating our algorithm right from the basics for arbitrary measurement locations avoids the need of interpolating the data to get a regular grid.

In order to do any reconstruction of the grain structure from individual orientation data we clearly need some modeling assumptions. For our algorithm we assume the following:

1. The domain is completely decomposed into grains which are separated by grain boundaries.
2. Grain boundaries are located at the bisectors of adjacent measurements locations.
3. There is a grain boundary between two adjacent measurement locations, if and only if, they belong to different phases or their misorientation angle exceeds a threshold given by the user.

Clearly, the first assumption may not be satisfied due to several reasons, e.g. a glassy phase or a highly distorted crystalline phase may occur at the grain boundaries or there might occur other amorphous regions. In such a case we assign a null phase to those regions and

* Corresponding author.
E-mail address: ralf.hielscher@mathematik.tu-chemnitz.de (R. Hielscher).

0304-3991/$ - see front matter © 2011 Elsevier B.V. All rights reserved.
doi:10.1016/j.ultramic.2011.08.002

treat them as an separate phase. This allows us to stay in the above framework. As for the third assumptions the crucial question is how to choose the threshold angle to model physically meaningful grain boundaries. Usually, the choice of the threshold is related to the definition of a small- or large-angle grain boundary, respectively (cf. [4]).

Based on the above modeling assumptions we straightforward derive a characterization of the reconstructed grains as compositions of Voronoi cells corresponding to the measurement locations x_ℓ, $\ell = 1,\dots,L$. With this characterization the outline of algorithm becomes obvious: First we perform a Voronoi decomposition of the domain corresponding to the measurement locations which results in a list of Voronoi cells D_ℓ, $\ell = 1,\dots,L$. Then we join all Voronoi cells which have a common face such that the phase on both sides of the face is the same and the misorientation is smaller than the threshold. The resulting compositions of Voronoi cells are the reconstructed grains. In the present paper we give a precise description of reconstruction algorithm as well as of constitutive algorithms for the computation of grain boundaries or grain volumes.

Functions of grain detection are included in commercial software packages which usually come with the EBSD hardware. Often, they act like black boxes, suffer from restrictions like a regular 2d grid of measurement locations which in turn requires some provision for missing data, cannot be well controlled or changed by the user, and do not allow for a simple generalization from 2d to 3d because of their ad hoc approach. On the other hand there are some algorithms described in the literature [5–8]. However, most of them lack a easily accessible implementation. The main advantages of the algorithm presented in this paper are

- The algorithm applies without any substantial modification to 2d as well as to 3d data.
- There is no need to interpolate missing orientation data or to infer them from their neighbors.
- Regions of missing orientation data are equally assigned to the neighboring grains.
- The assignment of the regions of missing orientations is invariant with respect to rotations and shifts of the specimen, i.e., rotations and shifts of the specimen result in accordingly rotated and shifted reconstructed grains.
- There is no systematic bias in the assignment of regions of missing orientations towards certain grains or phases.
- Missing orientations do not cause grains to be split into two grains. There is no need of joining them afterwards.
- Measurements resulting in very small grains, i.e., likely to indicate erroneous measurements, can be removed and the corresponding region can be assigned in an analogous way as regions of missing data.
- Large regions of missing data or subdomains of specific shape can be marked to be excluded from the grain reconstruction.
- The algorithms used in MTEX are fast as they scale almost linearly with the number of measured individual orientations, and stable as they are based upon well established and highly optimized and parallelized algorithms like for Voronoi decomposition and spanning tree.

This paper is aimed as a reference paper for earth- and material scientists who want to use the texture analysis software MTEX to analyze the microstructure of aggregates by means of individual orientation measurements. MTEX is a comprehensive, freely available MATLAB toolbox that covers a wide range problems of quantitative texture analysis, e.g. ODF modeling [9], pole figure to ODF inversion [10], ODF estimation from individual orientation measurements [11], computation of anisotropic material properties [12], statistics of individual orientation measurements [14]. The MTEX toolbox can be downloaded for free from http://mtex.googlecode.com. Unlike many other texture analysis software, it offers a programming interface, which allows for the efficient processing of involved research problems in the form of scripts (m-files). In MTEX texture information, like ODFs, EBSD data, pole figures, reconstructed grains are represented by variables of different types. For example in order to define a unimodal ODF with half-width 10°, preferred orientation (10°,20°,30°) Euler angles and cubic crystal symmetry, one issues the command

```
myODF = unimodalODF(orientation('Euler',10*degree,20*degree,30*degree),...
                    symmetry('cubic'),'halfwidth',10*degree)
```

which generates a variable myodf of type ODF which is displayed as

```
myODF = ODF
  specimen symmetry: triclinic
  crystal symmetry : cubic

  Radially symmetric portion:
    kernel: de la Vallee Poussin, hw = 10
    center: (10,20,30)
    weight: 1
```

We will keep this style of displaying input and output to make the syntax of MTEX as clear as possible. Note that there is also an exhaustive interactive documentation included in MTEX, which explains the syntax of each command in detail.

Our paper is organized as follows. In the first section we elaborate formally on graphs, cellular partitions, and Voronoi partition to develop the data model and algorithms to encode it. In the second section we derive our grain model from the modeling assumptions and formulate the algorithms for the grain reconstruction. We also present some subsequent algorithms for the calculation of the grain boundaries, the sub-grain boundaries and the grain volume. In the last section we apply our algorithm to a 2d data set and a 3d data set, respectively. The 2d data set was sampled from a surface of a layered (proto-)mylonite from the Western Gneiss Province, Norway, with a FEI Q400 FEG Scanning Electron Microscope equipped with a HKL Electron Backscatter Diffraction Facility at the University of California, Santa Barbara, USA, by Brad Hacker and Daniel Rutte. The 3d EBSD data were collected from a low-carbon steel specimen with a dual beam FIB (focused ion beam) scanning electron microscope of the type FEI NOVA600-Nanolab(r). The data were recorded at the Materials Science and Engineering Department of Ghent University by the group of Kestens and Petrov, cf. [15–17].

Once grain boundaries and grains are reconstructed, MTEX can be utilized to compute a wide variety of properties describing the microstructure of the aggregate, e.g.

- summary statistics of the total number of measurements, per phase, per grain, the total number of adjacent grains,
- join-count statistics of phase transitions for adjacent grains,
- distribution of grain size, grain shape, and boundary size,
- directional distribution of grain boundaries,
- orientation distribution analysis per grain,
- various kinds of misorientation distributions,
- characteristics of boundaries in terms of phase boundaries, large angle vs. small angle boundaries, twin boundaries,
- etc.

2. Graphs, polyhedra, and partitions

In this section we briefly present the mathematical terms required for our grain reconstruction algorithm.

2.1. Graphs

Since our data model for crystallographic grains is based on graphs we present here some basic notions of graph theory with special emphasis on incidence and adjacency matrices.

By a *graph* (V,E) we understand a finite set of vertices $V=\{v_1,\dots,v_I\}$ and a finite set of edges $E=\{e_1,\dots,e_J\}$ connecting some of the vertices. In this paper we restrict ourself to simple graphs, i.e., between two vertices there is at most one edge, all the edges are undirected, and there are no loops in the graph. More precisely, we want a graph to be identified with a symmetric $I\times I$ adjacency matrix $\mathcal{A}_V$ describing which vertices of the graph are connected by an edge, i.e., for $i,i'=1,\dots,I$:

$$[\mathcal{A}_V]^{i,i'}=\begin{cases}1 & \text{if } i\neq i' \text{ and the vertices } v_i \text{ and } v_{i'} \text{ are connected by an edge in } E,\\ 0 & \text{otherwise.}\end{cases}$$

An alternative but equivalent representation of a graph is its $I\times J$ incidence matrix $\mathcal{I}_{VE}$, which describes which vertices belongs to which edges, i.e., for $i=1,\dots,I$, and $j=1,\dots J$:

$$[\mathcal{I}_{VE}]^{i,j}=\begin{cases}1 & \text{if } v_i \text{ is a vertex of the edge } e_j,\\ 0 & \text{otherwise.}\end{cases}$$

Since every edge connects two vertices, every column of $\mathcal{I}_{VE}$ contains exactly twice the value 1. Furthermore, we have the following relationship to the adjacency matrix $\mathcal{A}_V$ of the graph:

$$[\mathcal{A}_V]^{i,j}=\begin{cases}[\mathcal{I}_{VE}\mathcal{I}_{VE}^T]^{i,j} & \text{if } i\neq j,\\ 0 & \text{if } i=j,\end{cases}$$

where $\mathcal{I}_{VE}^T$ denotes the transposed of the incidence matrix $\mathcal{I}_{VE}$.

A sequence of vertices $(v_{i_1},v_{i_2},\dots,v_{m_N})$ which are pairwise connected by edges, i.e., $\mathcal{A}_V^{i_n,i_{n+1}}=1$, $n=1,\dots,N-1$, is called a *path* in the graph. Two arbitrary vertices v_i and $v_{i'}$ in V are called *connected* if there is a path $(v_i=v_{i_1},v_{i_2},\dots,v_{i_N}=v_{i'})$ in the graph connecting the vertices. A graph (V,E) is called *connected* if any two vertices of the graph are connected.

Let (V,E) be a graph. A graph $(\tilde{V},\tilde{E})$ is called *subgraph* of (V,E) if $\tilde{V}\subset V$ and $\tilde{E}\subset E$. The subgraph $(\tilde{V},\tilde{E})$ is called a *connected component* of the graph (V,E) if it is connected and there is no other vertex in $V\backslash\tilde{V}$ that is connected to an vertex in $\tilde{V}$. In other word the connected components of a graph are its maximum connected subgraphs.

Statement 1. *For any graph (V,E) there is a well defined decomposition into connected components (V_m,E_m), $m=1,\dots,M$, such that the vertices V are the disjointed union of the vertices V_m and the edges E are the disjointed union of the edges E_m. The decomposition is uniquely described by the corresponding $I\times M$ incidence matrix $\mathcal{I}_{VC}$:*

$$[\mathcal{I}_{VC}]^{i,m}=\begin{cases}1 & \textit{if } v_i \textit{ is a vertex of the m-th component, i.e. } v_i\in V_m,\\ 0 & \textit{otherwise.}\end{cases}$$

This incidence matrix can be numerically computed by a standard depth-first or breadth-first search algorithm cf. [18, pp. 20, 319].

2.2. Polygons and polyhedra

Since the grains to be reconstructed by our algorithm will be composed of convex polygons or polyhedra, we present in this sections some basic facts and notations of these geometrical objects.

Let $d>0$ be an arbitrary dimension and let $v_1,\dots,v_I\in\mathbb{R}^d$ be a finite set of vertices. Then its *convex hull* $\mathrm{conv}(v_1\dots,v_I)\subset\mathbb{R}^d$ is defined as the set

$$\mathrm{conv}(v_1\dots,v_I)=\left\{v=\sum_{i=1}^{I}\lambda_i v_i \,\middle|\, \lambda_i>0 \text{ and } \sum_{i=1}^{I}\lambda_i=1\right\},$$

which can be interpreted as the smallest convex set enclosing $v_1,\dots,v_I$.

In the special case that the convex hull $\mathrm{conv}(v_1 \dots, v_I)$ is two-dimensional it is called *polygon*, if it is three-dimensional it is called *polyhedron*. The boundary of a polyhedron consists of polygons called *faces* and the boundary of polygons consists of edges.

The topological relationships between the vertices v_i, $i=1,\dots,I$, edges e_j, $j=1,\dots J$, and faces f_k, $k=1,\dots,K$, of a polyhedron can be represented by incidence matrices, i.e., by the matrices

$$[\mathcal{I}_{VE}]^{i,j} = \begin{cases} 1 & \text{if } v_i \text{ is a vertex of edge } e_j, \\ 0 & \text{otherwise} \end{cases}$$

and

$$[\mathcal{I}_{EF}]^{j,k} = \begin{cases} 1 & \text{if } e_j \text{ is edge of the face } f_k, \\ 0 & \text{otherwise.} \end{cases}$$

With these notations it is straight forward to compute the incidence matrix between vertices and faces of a polyhedron:

$$[\mathcal{I}_{VF}]^{ik} = [\mathcal{I}_{VE}\mathcal{I}_{EF}]^{i,k} = \begin{cases} 1 & \text{if } v_i \text{ is a vertex of the face } f_k, \\ 0 & \text{otherwise.} \end{cases}$$

Next we are interested in the volume of polytopes. First we consider the simple case of vertices $v_1, \dots, v_I \in \mathbb{R}^2$ in the plane defining a polygon. Then its area A is given by

$$A(x_1, \dots, x_I) = \left| \sum_{i=1}^{I} (v_i^x + v_{i+1}^x)(v_{i+1}^y - v_i^y) \right|.$$

In the case of vertices $v_1, \dots, v_I \in \mathbb{R}^3$ in the three-dimensional Euclidean space defining a polygon, its area is given by

$$A(v_1, \dots, v_I) = \frac{I}{2}(v_1 \times v_2 + v_2 \times v_3 + \dots + v_{I-1} \times v_{I+} v_I \times v_1).$$

Using these formulae the volume of a convex polyhedron with vertices v_i and faces f_k, $k=1,\dots,K$ can be computed by

$$V(v_1, \dots, v_I) = \frac{1}{3} \sum_{k=1}^{K} A(f_k)\ \mathrm{dist}(v_1, f_k).$$

2.3. The Voronoi decomposition

In this section we define the Voronoi decomposition [19,20] of a polyhedron $D \subset \mathbb{R}^3$ with respect to a finite set of distinct points in $x_1, x_2 \dots, x_L \in D$, $L \geq 2$. We restrict ourself to the three dimensional case only, since the two dimensional case is quite similar.

First, we define for any pair of points $x_\ell, x_{\ell'}$, $1 \leq \ell \neq \ell' \leq L$, the *half plane*

$$H(x_\ell, x_{\ell'}) = \{x \in D \,|\, \|x - x_\ell\| \leq \|x - x_{\ell'}\|\}, \tag{1}$$

which consists of all points in D which are closer to x_ℓ than to $x_{\ell'}$, and the *bisector*

$$b(x_\ell, x_{\ell'}) = \{x \in D \,|\, \|x - x_\ell\| = \|x - x_{\ell'}\|\}, \tag{2}$$

which consists of all points equidistant to x_ℓ and $x_{\ell'}$. Then for any point x_ℓ, $\ell = 1, \dots, L$, the corresponding *Voronoi cell* D_ℓ is defined as

$$D_\ell = D(x_\ell) = \bigcap_{\ell' \neq \ell} H(x_\ell, x_{\ell'}) = \{x \in D \,|\, \|x - x_\ell\| \leq \|x - x_{\ell'}\| \text{ for all } \ell' \neq \ell\}.$$

The set of all Voronoi cells D_ℓ, $\ell = 1, \dots, L$, associated to the point set $\{x_1, x_2 \dots, x_L\}$ is called *Voronoi decomposition* of D. It has the following properties:

1. Each Voronoi cell is a polyhedron.
2. The Voronoi cells cover the entire domain, i.e., $D = \bigcup_{\ell=1}^{L} D_\ell$.
3. The disjoint of two Voronoi cells is either empty, a vertex, an edge, or a face of both cells.

Since each Voronoi cell is a polytope the topological structure of a Voronoi decomposition D_ℓ, $\ell = 1, \dots, L$, can be described in terms of incidence matrices. Let v_i, $i=1,\dots,I$, be the vertices, e_j, $j=1,\dots J$, the edges, and f_k, $k=1,\dots,K$, the faces of the Voronoi cells. Then the topological structure of the Voronoi cells is described by incidence matrices

- $\mathcal{I}_{VE} \in \mathbb{R}^{I \times J}$—describing which vertices belong to which edge,
- $\mathcal{I}_{EF} \in \mathbb{R}^{J \times K}$—describing which edges belong to which face,
- $\mathcal{I}_{FD} \in \mathbb{R}^{K \times L}$—describing which faces belong to which Voronoi cell.

Two Voronoi cells are called *adjacent* if they have a common face. Hence, the $L \times L$ adjacency matrix $\mathcal{A}_D$ of the Voronoi cells is given by

$$[\mathcal{A}_D]^{\ell,\ell'} = \begin{cases} [\mathcal{I}_{FD}^T \mathcal{I}_{FD}]^{\ell,\ell'} & \text{if } \ell \neq \ell', \\ 0 & \text{if } \ell = \ell'. \end{cases}$$

In MTEX the QHULL library [21] which is part of MATLAB is used for the computation of the Voronoi decomposition.

3. The grain–grain boundary reconstruction scheme

In this section we describe our novel grain data model and reconstruction scheme. First, we explicitly state the model assumptions leading to our reconstruction scheme, and then we derive a geometrical characterization of the resulting grains.

3.1. Model assumptions and formal grain characterization

EBSD data are spatially referenced measurements of crystallographic orientations, i.e., they consists of triples (x_ℓ,o_ℓ,p_ℓ), $\ell=1,\dots,L$, of locations $x_\ell \in D \subset \mathbb{R}^3$, phase information p_ℓ, and orientations $o_\ell \in \mathrm{SO}(3)/\tilde{G}^{p_\ell}_{\mathrm{Laue}}$, where $\tilde{G}^{p_\ell}_{\mathrm{Laue}} \subset \mathrm{SO}(3)$ denotes the reduced Laue group of the phase p_ℓ. Our objective is to reconstruct the crystal grains from these data, i.e., the grains, the grain boundaries, and adjacency relationships between them. Our reconstruction scheme is based on the three modeling assumptions which we have already discussed in Introduction.

1. The domain is completely decomposed into grains which are separated by grain boundaries.
2. Grain boundaries located at the bisectors of adjacent measurement locations.
3. There is a grain boundary between two adjacent measurement locations, if and only if, they belong to different phases or their misorientation angle exceeds a threshold given by the user.

Let D_ℓ, $\ell=1,\dots,L$, be the Voronoi decomposition with respect to the measurement locations x_ℓ. Since the boundaries of the Voronoi cells are segments of the bisectors between adjacent measurement locations we conclude from model assumption 2 that the reconstructed grain boundaries are allowed only at the boundaries of the Voronoi cells D_ℓ. By assumption 1, the reconstructed grains are regions which are completely enclosed by grain boundaries and hence compositions of Voronoi cells D_ℓ. Together with assumption 3, we end up with the following definition of the grains of our reconstruction scheme:

Statement 2. *A grain $G \subset D$ is a composition of Voronoi cells D_ℓ such that*:

1. *Each pair of adjacent Voronoi cells which belongs to the same phase and has a misorientation angle smaller then the threshold is either completely contained in the grain or completely outside the grain.*
2. *There is no non-trivial subset of G satisfying condition*1.

An immediate feature of our reconstruction scheme is its invariance with respect to geometrical transformations, i.e., rotating and shifting the specimen rotates and shifts the reconstructed grains accordingly. Furthermore, it is independent of any measurement geometry, i.e., the measurements locations may be on an arbitrary grid.

3.2. Numerical implementation

In this section we describe the numerical implementation of our grain reconstruction scheme. We present our algorithm only for the three-dimensional case. The reduction to the two-dimensional case is straight forward. We start with a list of triples (x_ℓ,p_ℓ,o_ℓ), $\ell=1,\dots,L$, of locations $x_\ell \in D \subset \mathbb{R}^3$, phase information p_ℓ, and orientations $o_\ell \in \mathrm{SO}(3)/\tilde{G}^{p_\ell}_{\mathrm{Laue}}$, where $\tilde{G}^{p_\ell}_{\mathrm{Laue}} \subset \mathrm{SO}(3)$ denotes the reduced Laue group of phase p_ℓ. In order to illustrate our grain reconstruction scheme we consider a two dimensional example as displayed in Fig. 1, where orientations are displayed as directions for simplicity.

Step 1 – Voronoi decomposition: In the first step the Voronoi decomposition D_ℓ, $\ell=1,\dots,L$, of the measurement locations x_ℓ is computed, cf. Fig. 2. It results in a list of vertices v_i, $i=1,\dots,I$, a list of edges e_j, $j=1,\dots,J$, a list of faces f_k, $k=1,\dots,K$, and the corresponding incidence matrices $\mathcal{I}_{VE}$, $\mathcal{I}_{EF}$, $\mathcal{I}_{FD}$. The Voronoi decomposition of our illustrative example is shown in Fig. 2.

Using these incidence matrices it is straight forward to compute the $L \times L$ adjacency matrix $\mathcal{A}_D$:

$$[\mathcal{A}_D]^{\ell,\ell'} = \begin{cases} [\mathcal{I}_{FD}^T \mathcal{I}_{FD}]^{\ell,\ell'}, & \text{if } \ell \neq \ell', \\ 0, & \text{if } \ell = \ell', \end{cases}$$

which satisfies $\mathcal{A}_D^{\ell,\ell'}=1$ whenever the two Voronoi cells D_ℓ and $D_{\ell'}$ share a common face. Thus the adjacency matrix $\mathcal{A}_D$ records which of the measurements locations are adjacent, i.e., the position of potential grain boundaries. These neighborhood relationships are illustrated in Fig. 3.

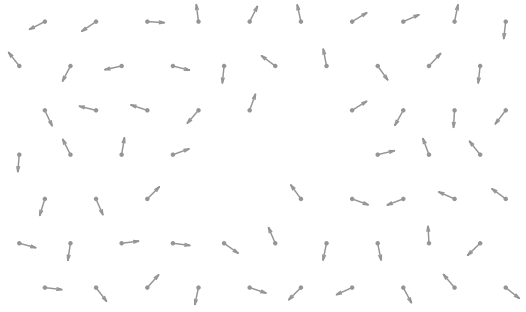

Fig. 1. Orientation data $o_\ell, \ell=1,\dots,L$, on an initially regular hexagonal grid with missing data: For simplicity the orientations are considered only in 2d and are displayed by arrows. Because of the missing data the measurements are no longer arranged according to a regular grid.

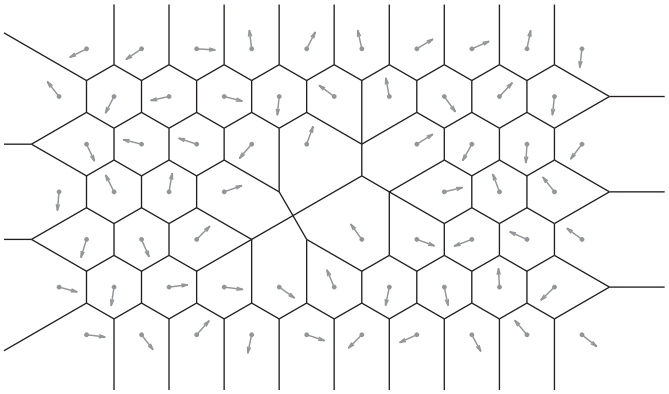

Fig. 2. The Voronoi decomposition of the measurement locations.

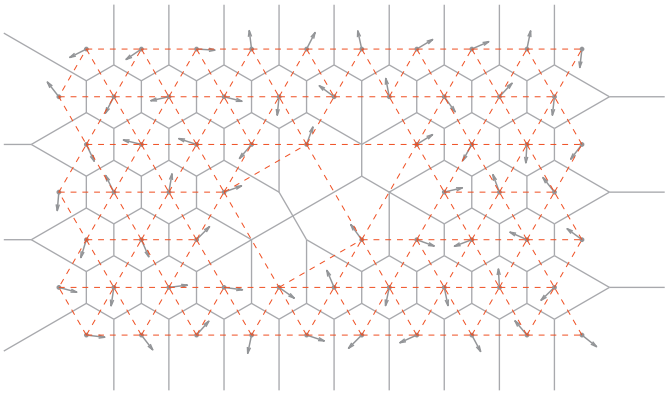

Fig. 3. The Voronoi decomposition of the measurement locations with neighboring Voronoi cells linked by hatched red lines. These red links correspond to the ones in the adjacency matrix $\mathcal{A}_D$. (For interpretation of the references to color in this figure legend, the reader is referred to the web version of this article.)

Step 2 – Grain boundaries: In the second step it is checked whether a common face between two adjacent Voronoi cells is an actual grain boundary. Let $D_\ell, D_{\ell'}$ be two adjacent Voronoi cells. Then their common face is a grain boundary, if and only if the corresponding phases p_ℓ and $p_{\ell'}$ are different or the misorientation angle:

$$d(o_\ell, o_{\ell'}) = \min_{\sigma \in \tilde{G}^{\tilde{P}_\ell}_{\mathrm{Laue}}} \omega(o_\ell^{-1} o_{\ell'} \sigma) > \delta$$

exceeds a given threshold angle δ. According to this criterion we decompose the adjacency matrix $\mathcal{A}_D$ into two matrices:

$$\mathcal{A}_D = \mathcal{A}_D^+ + \mathcal{A}_D^-,$$

which are defined as

$$[\mathcal{A}_D^+]^{\ell,\ell'} = \begin{cases} 1 & \text{if } A^{\ell,\ell'} = 1 \text{ and } p_\ell = p_{\ell'} \text{ and } d(o_\ell, o_{\ell'}) \le \delta, \\ 0 & \text{otherwise} \end{cases}$$

and

$$[\mathcal{A}_D^-]^{\ell,\ell'} = \begin{cases} 1 & \text{if } A^{\ell,\ell'} = 1 \text{ and } p_\ell \neq p_{\ell'} \text{ or } d(o_\ell, o_{\ell'}) > \delta, \\ 0 & \text{otherwise.} \end{cases}$$

Defined in this way the matrix $\mathcal{A}_D^+$ contains all neighborhood relationships between Voronoi cells which have a common face that is not an grain boundary, and $\mathcal{A}_D^-$ contains all neighborhood relationships between Voronoi cells which have a common face that is a grain boundary. This is illustrated in Fig. 3.

Step 3 – Grains: In the third step we consider the graph with vertices x_ℓ, $\ell = 1, \ldots, L$, given by the measurements, and edges connecting exactly those vertices such that the corresponding Voronoi cells have a common face that is not a grain boundary. The adjacency matrix of this graph is the matrix $\mathcal{A}_D^+$ defined in Step 2. According to our grain characterization in Statement 1, two measurements locations $x_\ell, x_{\ell'}$ belong to the same grain, if and only if x_ℓ and $x_{\ell'}$ belong to the same connected component of the graph given by $\mathcal{A}_D^+$ (Fig. 4).

In order to compute all connected components of the graph given by $\mathcal{A}_D^+$ we apply a standard depth-first or breadth-first search algorithm. cf. [18, pp. 20, 319]. As a result we obtain an $L \times M$ incidence matrix $\mathcal{I}_{DG}$ that describes the connected components by

$$[\mathcal{I}_{DG}]^{\ell,m} = \begin{cases} 1 & \text{if the measurement location } x_\ell \text{ belongs to the } m\text{-th component,} \\ 0 & \text{otherwise.} \end{cases}$$

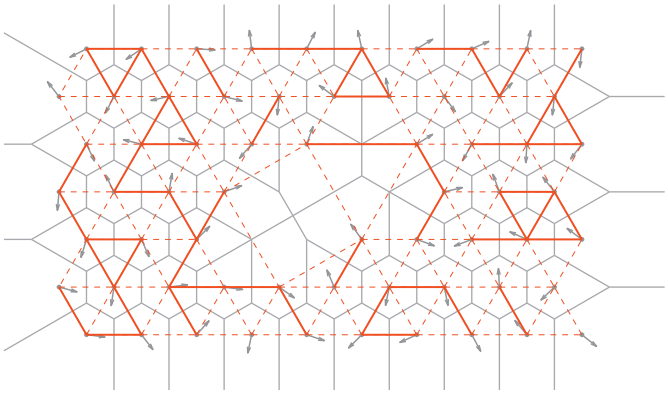

Fig. 4. In this figure adjacent measurements that are not separated by a grain boundary are linked by bold red lines. These bold red lines form the graph represented by the adjacency matrix $\mathcal{A}_D^-$. (For interpretation of the references to color in this figure legend, the reader is referred to the web version of this article.)

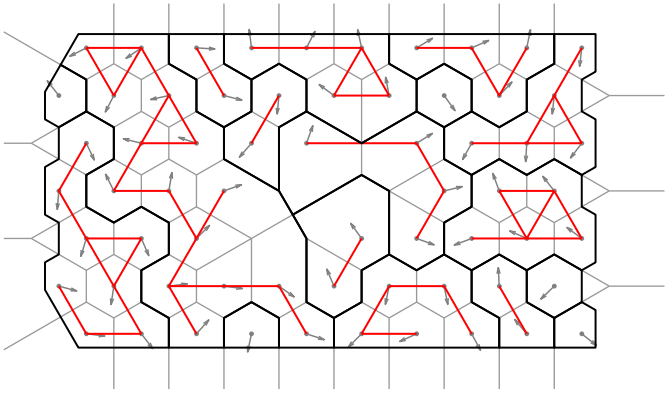

Fig. 5. The components of the graph defined by $\mathcal{A}_D^-$ as well as the corresponding grains g_m, $m=1,\dots,M$.

Using again our grain characterization in Statement 1 we conclude that the M connected components define M grains $g_m \subset D$, $m=1,\dots,M$, by

$$g_m = \bigcup_{\substack{\ell=1,\dots,L \\ I_{\ell,m}=1}} D_\ell.$$

With this definition the incidence matrix $\mathcal{I}_{DG}$ may be interpreted as

$$[\mathcal{I}_{DG}]^{\ell,m} = \begin{cases} 1 & \text{if the Voronoi cell } D_\ell \text{ belongs to the grain } g_m, \\ 0 & \text{otherwise.} \end{cases}$$

Hence, we end up with a grain model for the EBSD measurements (x_ℓ, p_ℓ, o_ℓ), $\ell = 1,\dots,L$. The components of the graph as well as the grains g_m, $m=1,\dots,M$, are illustrated in Fig. 5.

3.3. Basic grains properties

In this section we discuss the implementation of various topological and geometrical properties to our grain model.

Grain neighborhood relationships: We start by computing the neighborhood relationships between the reconstructed grains. These neighborhood relationships are described by an $M \times M$ adjacency matrix $\mathcal{A}_G$:

$$[\mathcal{A}_G]^{m,m'} = \begin{cases} 1 & \text{the grains } g_m \text{ and } g_{m'} \text{ have a common grain boundary,} \\ 0 & \text{otherwise.} \end{cases}$$

Given the matrixes $\mathcal{A}_D^-$ and $\mathcal{I}_{DG}$ computed in Step 3 we have

$$[\mathcal{A}_G]^{m,m'} = \begin{cases} 1 & \text{if } [\mathcal{I}_{DG}^T \mathcal{A}_D^- \mathcal{I}_{DG}]^{m,m'} \geq 1, \\ 0 & \text{otherwise.} \end{cases}$$

Grain boundaries: Next we want to identify grain boundaries and sub-grain boundaries. Therefore, we consider the matrix:

$$\mathcal{B}_D = \mathcal{I}_{DG} \mathcal{I}_{DG}^T,$$

which records whether two Voronoi cells belong to the same grain, i.e.,

$$[\mathcal{B}_D]^{\ell,\ell'}\begin{cases}1 & \text{if the Voronoi cells } D_\ell \text{ and } D_{\ell'} \text{ belong to the same grain,}\\ 0 & \text{otherwise.}\end{cases}$$

Let us remember that the matrix $\mathcal{A}_D^-$ describes the grain boundaries between adjacent Voronoi cells. In order to distinguish grain boundaries and sub-grain boundaries we multiply the matrix $\mathcal{A}_D^-$ element-wise with the matrix $\mathcal{B}_D$, i.e.,

$$\mathcal{A}_D^{\text{sub}} = \mathcal{A}_D^- \odot \mathcal{B}_D.$$

Then $[\mathcal{A}_D^{\text{sub}}]^{\ell,\ell'} = 1$ indicates that the common face of the Voronoi cells D_ℓ and $D_{\ell'}$ is an sub-grain boundary. The complement of $\mathcal{A}_D^{\text{sub}}$ with respect to $\mathcal{A}_D^-$

$$\mathcal{A}_D^{\text{boundary}} = \mathcal{A}_D^- - \mathcal{A}_D^{\text{sub}}$$

describes the ordinary grain boundaries, i.e., $[\mathcal{A}_D^{\text{boundary}}]^{\ell,\ell'} = 1$ indicates that the common face of the Voronoi cells D_ℓ and $D_{\ell'}$ is a grain boundary.

Finally, we set up an incidence matrices $\mathcal{I}_{FG}^{\text{boundary}}$, $\mathcal{I}_{FG}^{\text{sub}}$ answering the question whether a face is a boundary or sub-boundary of a specific grain, i.e.,

$$[\mathcal{I}_{FG}^{\text{boundary}}]^{k,m} = \begin{cases}1 & \text{if face } f_k \text{ belongs to the grain boundary of grain } g_m,\\ 0 & \text{otherwise}\end{cases},$$

and

$$[\mathcal{I}_{FG}^{\text{sub}}]^{k,m} = \begin{cases}1 & \text{if face } f_k \text{ belongs to the sub grain boundary of grain } g_m,\\ 0 & \text{otherwise.}\end{cases}$$

These incidence matrices can be effectively computed via

$$\mathcal{I}_{FG}^{\text{boundary}} = \mathcal{I}_{FD}\mathcal{A}_D^{\text{boundary}}\mathcal{I}_{DG} \odot (\mathcal{I}_{FD}\mathcal{I}_{DG}),$$

$$\mathcal{I}_{VG}^{\text{sub}} = \mathcal{I}_{FD}\mathcal{A}_D^{\text{sub}}\mathcal{I}_{DG} \odot (\mathcal{I}_{FD}\mathcal{I}_{DG}),$$

where $\odot$ denotes the pointwise multiplication of the matrices. Fig. 6 displays this distinction between grain boundaries and sub-grain boundaries.

Grain boundary between selected grains: With the incidence matrix $\mathcal{I}_{FG}^{\text{boundary}}$ in place it is straight forward to compute for any two selected grains g_{m_1} and g_{m_2} its common grain boundary. More precisely, the common grain boundary can be represented by a binary vector $\mathcal{B}_F$ which indicates for each Voronoi face f_k whether it belongs to the common grain boundary or not, i.e.,

$$[\mathcal{B}_F]^k = \begin{cases}1 & \text{if face } f_k \text{ belongs to the grain boundary between grain } g_{m_1} \text{ and grain } g_{m_2},\\ 0 & \text{otherwise.}\end{cases}$$

The vector $\mathcal{B}_F$ is effectively computed by the formula:

$$[\mathcal{B}_F]^k = [\mathcal{I}_{FG}^{\text{boundary}}]^{k,m_1}[\mathcal{I}_{FG}^{\text{boundary}}]^{k,m_2}.$$

Geometrical properties: Since the grains are defined as compositions of polyhedra the computation of geometrical properties can be done by standard methods. Let us mention only the most important ones.

For the volume of a grain we compute first the volume $[V_D]^\ell$ of each Voronoi cell D_ℓ and store them as a vector $V_D = ([V_D]^1, \ldots, [V_D]^L)^T$. Then the volumes $[V_G]^m$, $m=1,\ldots,M$ of the grains g_m are given by the entries of the vector:

$$V_G = \mathcal{I}_{GD}V_D.$$

As a second example we consider the surface area of the grains. Therefore, we first compute the surface area $[S_F]^k$ of each face f_k of every Voronoi cell and store them as a vector $S_F = ([S_F]^1, \ldots, S_F^K)$. Then the surface areas $[S_G]^m$, $m=1,\ldots,M$ of the grains g_m are given by the

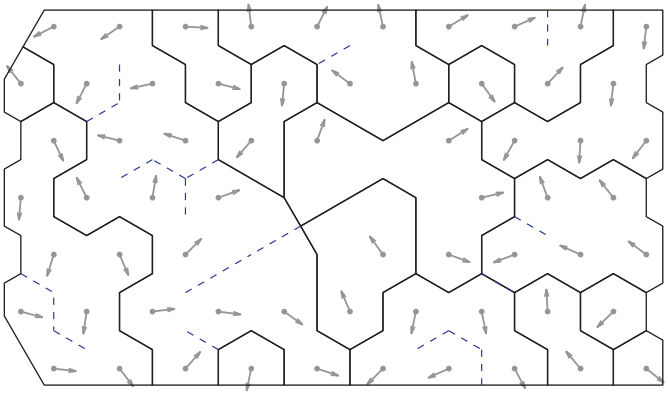

Fig. 6. Resulting partition displaying grain boundaries (black lines) and sub-grain boundaries (hatched blue lines). (For interpretation of the references to color in this figure legend, the reader is referred to the web version of this article.)

entries of the vector:

$$S_G = (\mathcal{I}_{FG}^{\text{boundary}})^t S_F,$$

where $(\mathcal{I}_{FG}^{\text{boundary}})^t$ denotes the transposed matrix to $\mathcal{I}_{FG}^{\text{boundary}}$.

4. Practical application to EBSD data

In this section our grain reconstruction algorithm is practically exemplified for a 2d and a 3d EBSD data set, respectively. All computations are done with our free and open Matlab ® toolbox MTEX 3.2 (cf. http://mtex.googlecode.com).

4.1. Practical application to a 2d EBSD data set

For a first illustration we use a 2d EBSD data set, which was sampled from a surface of a layered (proto-)mylonite from the Western Gneiss Province, Norway, with a FEI Q400 FEG Scanning Electron Microscope equipped with a HKL Electron Backscatter Diffraction Facility at the University of California, Santa Barbara, USA, by Brad Hacker and Daniel Rutte, at that time visiting graduate student form TU Bergakademie Freiberg. For additional details and a geologic interpretation we refer to a forthcoming publication by Rutte and Hacker. Orientation measurements were taken at locations of a square grid with 1000×280 points with a step size of 30 μm in both directions. The experiment is summarized in Table 1. Due to usual technical problems during the measurements indexing of the Kikuchi pattern failed for about 60.25% of all locations. Thus the data sets comprises about 112,000 valid orientation measurements only. This deficiency of the data set will be compensated by the Voronoi partition corresponding to the remaining locations of valid data.

In order to import the data into MTEX we have to specify the crystal symmetries of the phases present in the specimen first.

```
CS = {...
  symmetry('-1',[8.169,12.851,7.1124],[93.63,116.4,89.46]*degree,...
           'mineral','Andesina An28'),...
  symmetry('-3m',[4.913,4.913,5.504],'a//y',...
           'mineral','Quartz-new'),...
  symmetry('2/m',[5.339,9.249,20.196],[90,95.06,90]*degree,...
           'mineral','Biotite'),...
  symmetry('2/m',[8.5632,12.963,7.2099],[90,116.07,90]*degree,...
           'mineral','Orthoclase')};
```

Since the EBSD data are stored in a text file with columns for phase, Euler angles and spatial coordinates they can be imported by the generic EBSD interface of MTEX. The command to import the data is

```
ebsd = loadEBSD(fname, CS, 'ignorePhase', 0, ...
  'ColumnNames', {'index' 'Phase' 'x' 'y' 'Euler1' 'Euler2' 'Euler3' 'MAD'});
```

which results in a variable of type EBSD which is displayed as

```
ebsd = EBSD (P5629U1.txt)
  properties: index, mad
  phase orientations       mineral symmetry crystal reference frame
      1        43087 Andesina An28       -1             X||a*, Z||c
      2        37813    Quartz-new      -3m       X||a*, Y||b, Z||c
      3         3180       Biotite      2/m       X||a*, Y||b, Z||c
      4        27233    Orthoclase      2/m       X||a*, Y||b, Z||c
```

In order to plot a phase map of the data we issue the command

```
plot(ebsd,'property','phase')
```

The result is displayed in Fig. 7. The black rectangle with its lower left vertex at (19,000, 1500) and its upper right vertex at (23,000, 3,000) indicate a region of interest (RoI) where we want to analyze our data in greater detail. Such a region of interest can be defined by

```
region = polygon('rectangle',19000,1500,23000,3000)
```

Table 1
Summary of number of measurements N to area A relationship per phase.

Phase	N	%	Rel. %	A (μm)	%	Rel. density (%)
Not indexed	168,687	60.25				
Andesina	43,087	15.39	38.71	100.563×10^6	39.73	97.44
Quartz	37,813	13.50.9	33.97	87.766×10^6	34.67	97.98
Biotite	3180	1.14	2.86	8.924×10^6	3.53	81.03
Orthoclase	27,233	9.73	24.47	55.891×10^6	22.08	110.81
Total	280,000	(100)		253.145×10^6		100

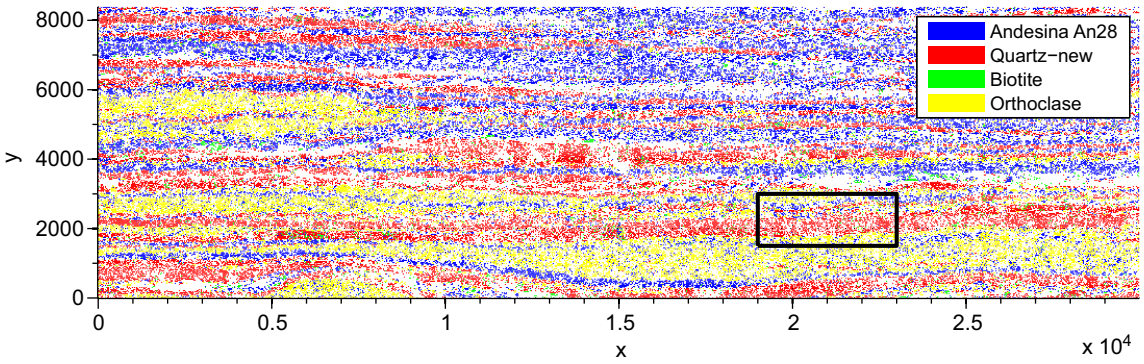

Fig. 7. Phase map of multi-phase rock specimen with Andesina (blue), Quartz (red), Biotite (green) and Orthoclase (yellow), the box is indicating a region of special interest (RoI). (For interpretation of the references to color in this figure legend, the reader is referred to the web version of this article.)

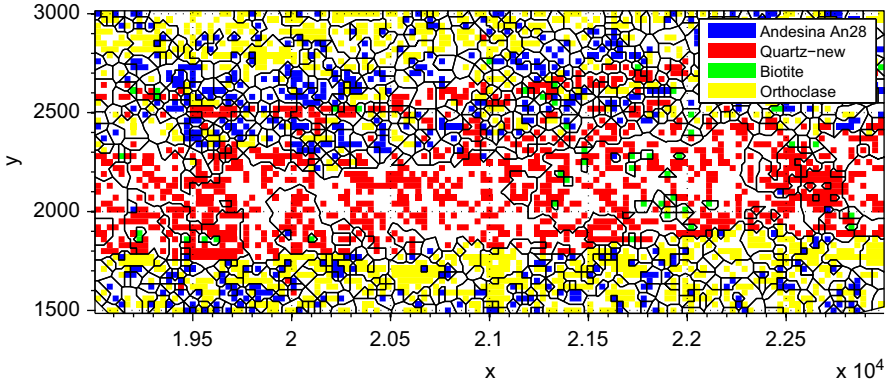

Fig. 8. (RoI) Detailed phase map with measurement locations and reconstructed grain boundaries.

The restriction of the EBSD data to this region can be computed by

```
ebsd_region = ebsd(region)
```

```
ebsd_region = EBSD (P5629U1.txt)
  properties: index, mad
  phase orientations       mineral symmetry crystal reference frame
      1          578 Andesina An28       -1             X||a*, Z||c
      2         1144    Quartz-new      -3m       X||a*, Y||b, Z||c
      3           58       Biotite      2/m       X||a, Y||b*, Z||c
      4         1066    Orthoclase      2/m       X||a*, Y||b, Z||c
```

Next we use our algorithm to reconstruct the grains and grain boundaries in the region of interest. The algorithm is started by the command `calcGrains` which involves the threshold angle δ as an optional argument.

```
grains = calcGrains(ebsd_region,'angle',15*degree)
```

```
grains = grain (from P5629U1.txt)
  phase grains       mineral symmetry crystal reference frame
      1    371 Andesina An28       -1             X||a*, Z||c
      2    189    Quartz-new      -3m       X||a*, Y||b, Z||c
      3     55       Biotite      2/m       X||a, Y||b*, Z||c
      4    381    Orthoclase      2/m       X||a*, Y||b, Z||c
```

The output is a variable of type `grain` which is a list of reconstructed grains. Now let us plot the grain boundaries in the region of interest as marked in Fig. 7 and overlay them with the phase information of the individual orientation measurements. With the commands `hold all` and `hold off` `MTEX` is told to overlay all figures to be plotted in between into one figure.

```
hold all
plot(ebsd_region,'property','phase')
plot(grains)
hold off
```

The result is displayed in Fig. 8. Obviously the extent of missing orientation data is not uniformly distributed throughout the region of interest but depends largely on the phase, cf. Table 1. Quartz seems to be most severely affected by missing data, while Orthoclase was

more successfully indexed than the average as realized for Andesina and Quartz. Thus, to the largest extent, Quartz grains to be determined will depend on the buffering of measurement locations to Voronoi cells.

Fig. 9 displays the reconstructed grain boundaries together with the individual orientation measurement of quartz and demonstrates that beside the large extend of missing data the modeled grains match the data. The plot was created with the commands

```
hold all
plot(grains({'An','Bi','Or'}),'property','phase','FaceAlpha',0.4)
plotBoundary(grains,'color','black');
plot(ebsd_region('Qu'))
hold off
colorbar
```

These commands exemplify how to use various options. By `grains({'An','Bi','Or'})` we select from all grains only those of phase Andesina, Biotite, and Orthoclase any by `ebsd_region('Qu')` we select only the EBSD data of phase Quartz. The option `FaceAlpha` can be used to shade down the output of the specific command. The EBSD measurements of the Quartz phase are colored according to their orientation, which in turn is color coded with respect to the color map provided by the (001) inverse pole figure (see Fig. 9b).

Next we want to plot the Quartz grains colored according to the mean orientation. This is done by the commands:

```
hold all
plot(grains({'An','Bi','Or'}),'property','phase','FaceAlpha',0.2)
plot(grains('Qu'))
hold off
colorbar
```

The result is shown in Fig. 10.

Once grain boundaries have been reconstructed, they may be classified according to some criteria, e.g. small vs. large angle boundaries by thresholding, or by checking the misorientation of adjacent grains for some specific relationships. In Fig. 11 grain

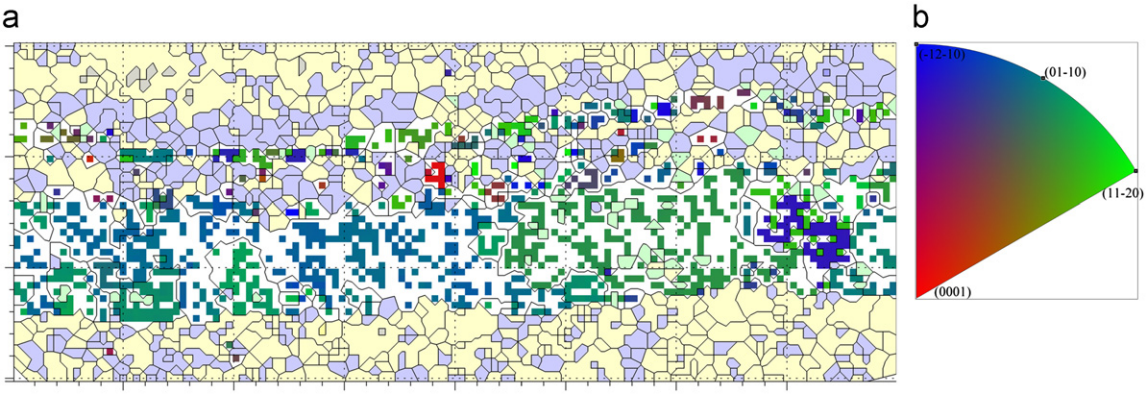

Fig. 9. (RoI) Individual orientation measurements of quartz together with the grain boundaries. (a) Orientation map. (b) Color map. (For interpretation of the references to color in this figure legend, the reader is referred to the web version of this article.)

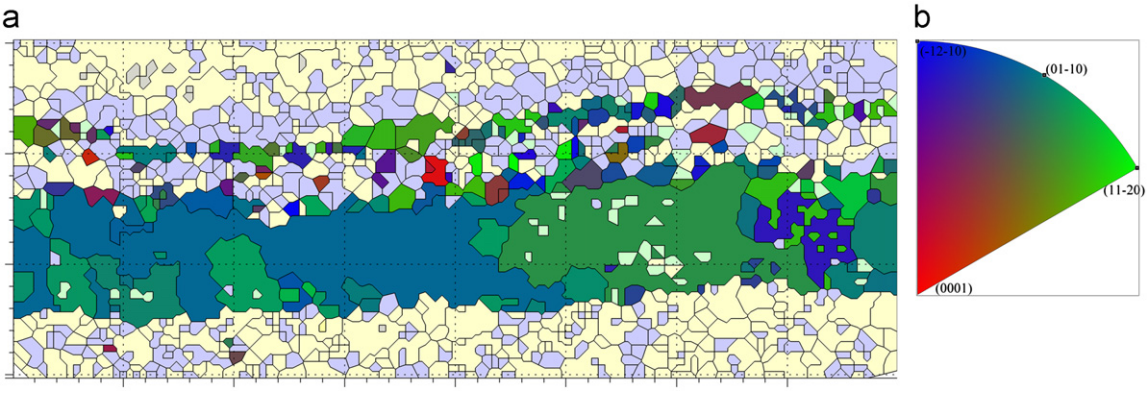

Fig. 10. (RoI) The reconstructed grains. The quartz grains are colored according to their mean orientation while the remaining grains are colored according to there phase. (a) Orientation map. (b) Color map.

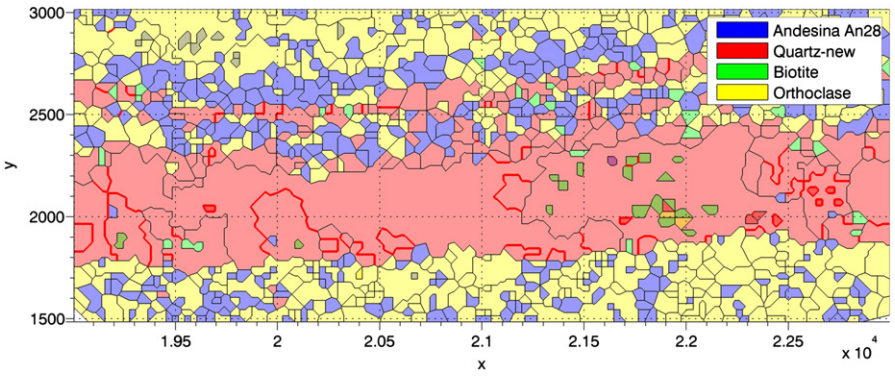

Fig. 11. (RoI *A*) Phase map with grain boundaries highlighted, where adjacent grains have a misorientation with rotational axis close to the *c*-axis.

boundaries are highlighted, where the misorientation of their adjacent grains is a rotation about the *c*-axis with an allowed tolerance of 5 degrees. Fig. 11 was accomplished with the commands

```
hold all
plot(grains,'property','phase','FaceAlpha',0.4)
plotBoundary(grains,'property',zvector,'delta',5*degree,'linewidth',2)
hold off
```

4.2. Practical application to a 3d EBSD data set

In this section we apply our algorithm to 3d EBSD data which were collected from a low-carbon steel specimen with a dual beam FIB (focused ion beam) scanning electron microscope of the type FEI NOVA600-Nanolab(r). The data were recorded at the Materials Science and Engineering Department of Ghent University by the group of Kestens and Petrov, cf. [15–17]. Orientation measurements were taken at locations of registered planar square grids with a stepsize of 0.1 μm in both directions and a spacing of equidistant planes of 0.12 μm. The data sets comprises $140 \times 160 \times 59$ orientation measurements. In order to import the data into MTEX we first specify the *z*-coordinates of the slices and then call the command `loadEBSD` with the name of the directory containing the data files.

```
hold all
plot(grains,'property','phase','FaceAlpha',0.4)
plotBoundary(grains,'property',zvector,'delta',5*degree,'linewidth',2)
hold off
```

```
z = (0:58)*0.12;
ebsd = loadEBSD('directoryName','3d', z)
```

```
ebsd = EBSD (S58.ANG)
  properties: ci, fit, iq, sem_signal
  phase orientations        mineral symmetry crystal reference frame
      1      1321600 Iron bcc (old)       43
```

The data can be visualized by plotting the individual orientations on slices passing through the measured cube. In MTEX this can be interactively done by the command

```
plot(ebsd)
```

The resulting plot is shown in Fig. 12a.

Since the data set is perfectly complete, computations to determine the 3d Voronoi cells is not required but instead partition into cube volume elements (“voxels”) applies. With the only difference that in this special case grains are composed of voxels, the determination of grains and grain boundaries is analogously to the two dimensional case.

```
grains = calcGrains(ebsd,'angle',10*degree,'unitcell');
```

```
grains = grain (from S58.ANG)
  phase grains        mineral symmetry crystal reference frame
      1   2233 Iron bcc (old)     m-3m
```

In order to visualize the grains we first restrict ourself to 43 mid-sized grains by

```
largeGrains = grains(grainSize(grains)>1000 & grainSize(grains)<100000);
```

```
largeGrains = grain (from S58.ANG)
  phase grains        mineral symmetry crystal reference frame
      1     43 Iron bcc (old)     m-3m
```

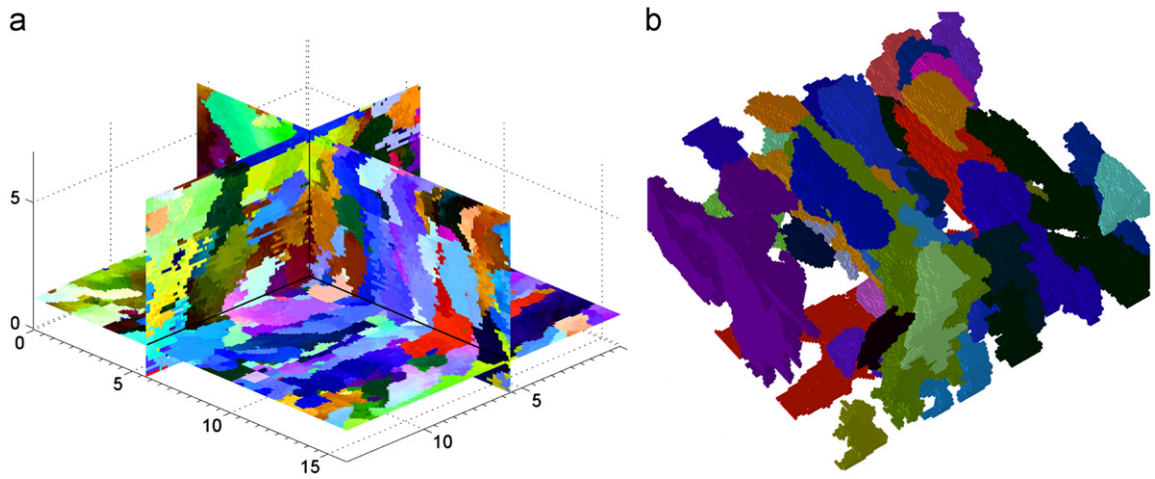

Fig. 12. View of 3d solid grain model based on EBSD data from serial sectioning (left), and slicing the 3d grain model (right). (a) Slices and (b) Grains.

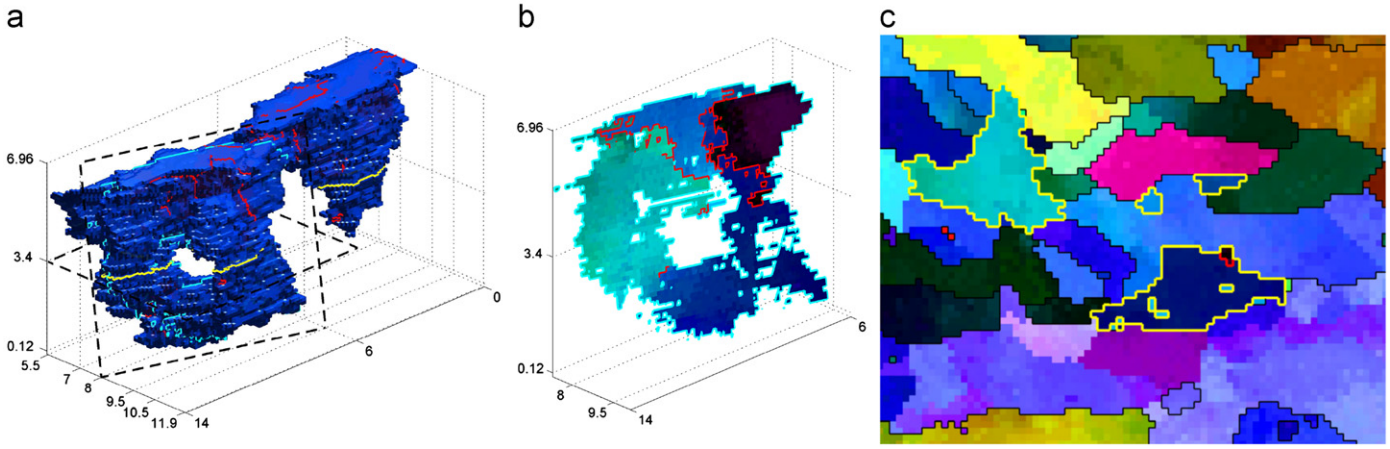

Fig. 13. View of an individual grain with sub-boundaries; lines of intersection of boundaries and sub-boundaries are marked in red, and two planes of sectioning are marked in cyan and yellow, respectively (left). While the section by the plane depicted in cyan suggests a set of adjacent grains (center), the section by the plane depicted in yellow indicates spatially separated grains (right). (a) 3d plot, (b) section A, (c) section B. (For interpretation of the references to color in this figure legend, the reader is referred to the web version of this article.)

Then we plot these grains by the command

```
plot(largeGrains)
```

The result is shown in Fig. 12b.

In Fig. 13 a single grain is plotted from different points of view. In Fig. 13a, a three 3d views of the grain are shown, whereas its intersections with two different planes are displayed in Fig. 13b and c. What appears as a hole in Fig. 13a of the 3d model makes the grain appear as two or more separated grains in Fig. 13c.

A completely worked out example considering 3d EBSD data will be included in the on-line documentation and ready for download. For the time being there is only little experience of interpretation and quantitative evaluation of 3d views of the fabric, e.g. with respect to the parametrization of grain boundaries in terms of location, crystallographic misorientation, and spatial orientation of the face by its unit normal vector. Future discussions within the texture and fabric community will clarify which properties derived from 3d EBSD data are crucial and how they should be visualized to facilitate expert interpretation and inference.

5. Conclusions

A novel general approach to grain boundary reconstruction based on explicit mathematical modeling assumptions and employing Voronoi decomposition of the domain of measurement locations has been presented. Its major advantages are that

- it applies to EBSD data in 2d or 3d domains,
- it is invariant with respect to translation and rotation of the specimen,
- it does not require interpolation of orientation measurements to substitute poorly indexed or missing orientation data,
- it is fast, i.e., the order of magnitude of computer time of the algorithms used in MTEX is almost linear.

Spatial modeling of grains and grain boundaries opens the route towards comprehensive fabric analysis as envisioned by Bruno Sander [22], e.g. it is a prerequisite of orientation statistics per grain as developed in [9], and to misorientation analysis with respect to neighboring grains, also included in MTEX. All computations are done with our free and open Matlab ® toolbox MTEX 3.2 [24].

Acknowledgments

The authors would like to thank Brad R. Hacker, Professor of Earth Science at the Earth Research Institute of the University of California, Santa Barbara, USA, and Daniel Rutte, TU Bergakademie Freiberg and former visiting graduate student at UC Santa Barbara, for the 2d EBSD data set of a mylonite, and Leo Kestens, Professor of Metal Science and Technology with the Department of Materials Science and Engineering at Ghent University, Belgium, for the 3d EBSD data set from a low-carbon steel specimen. The senior author (HS) would like to thank Fundação Coordenação de Aperfeiçoamento de Pessoal de Nível (CAPES) and German Academic Exchange Service (DAAD) for funding a three months research stay at Centro de Microscopia da Universidade Federal de Minas Gerais in Belo Horizonte, Brazil, with Prof. Karla Balzuweit and Prof. Carlos A. Rosière, during which this paper was completed.

References

[1] B.L. Adams, S.I. Wright, K. Kunze, Orientation imaging: The emergency of a new microscopy, Metallurgy Transactions 24A (1993) 819–831.
[2] K. Kunze, S.I. Wright, B.L. Adams, D.J. Dingley, Advances in automatic EBSP single orientation measurements, Textures and Microstructures 20 (1993) 41–54.
[3] A. Rollett, S. Lee, R. Campman, G. Roherer, Three dimensional characterization of microstructure by electron back-scatter diffraction, Annual Review of Material Research 37 (2007) 627–658.
[4] P.S. Bate, R.D. Knutsen, I.B. Rough, F.J. Humphreys, The characterization of low-angle boundaries by EBSD, Journal of Microscopy 220 (2005) 36–46.
[5] R. Heilbronner, Automatic grain boundary detection and grain size analysis using polarization micrographs or orientation images, Journal of Structural Geology 22 (2000) 969–981.
[6] Y. Li, C.M. Onasch, Y. Guo, GIS-based detection of grain boundaries, Journal of Structural Geology 30 (2008) 431–443.
[7] A.K. Kulshreshth, A. Alpers, T.G. Herman, E. Knudsen, L. Rodek, H.F. Poulsen, A greedy method for reconstructing polycrystals from three-dimensional x-ray diffraction data, Inverse Problems and Imaging 3 (2009) 69–85.
[8] A. Melcher, A. Unser, M. Reichhardt, B. Nestler, M. Pötschke, M. Selzer, Conversion of EBSD data by a quaternion based algorithm to be used for grain structure simulations, Technische Mechanik 30 (2010) 401–413.
[9] F. Bachmann, R. Hielscher, P.E. Jupp, W. Pantleon, S. Schaeben, E. Wegert, Inferential statistics of EBSD data from within individual crystalline grains, Journal of Applied Crystallography 43 (2010) 1338–1355.
[10] R. Hielscher, H. Schaben, A novel pole figure inversion method: specification of the MTEX algorithm, Journal of Applied Crystallography 41 (2008) 1024–1037.
[11] R. Hielscher, Kernel density estimation on the rotation group. Preprint 2010-7, FakultÃd't fÃijr Mathematik, TU Chemnitz, 2010.
[12] D. Mainprice, R. Hielscher, H. Schaeben, Calculating anisotropic physical properties from texture data using the MTEX open source package, Society, 1–33, in: D.J. Prior, E.H. Rutter, D.J Tatham (Eds.), Deformation Mechanisms, Rheology and Tectonics: Microstructures, Mechanics and Anisotropy, 360, Geological Society, London, 2011, pp. 175–192 doi: 10.1144/SP360.10 (Special publications).
[14] R. Hielscher, H. Schaeben, H. Siemes, Orientation Distribution Within a Single Hematite Crystal, Mathematical Geosciences 42 (2010) 375–395.
[15] R. Petrov, O.L. Garcia, J.J.L. Mulders, A.C. Reis, J.-H. Bae, L. Kestens, Y. Houbaert, Three dimensional microstructure-microtexture characterisation of pipeline steel, in: P.B. Prangnell, P.S. Bate (Eds.), Fundamentals of Deformation and Annealing, 550, Materials Science Forum, 2007, pp. 625–630.
[16] R. Petrov, O.L. Garcia, H. Sharma, P.G. Hernandez, L. Kestens, 3D-microstructure and texture characterization in different length scales, in: A.D. Rollet, (Ed.), Applications of Texture Analysis, Ceramic Transactions 201A, Collection of Papers Presented at the 15th International Conference on Texture in Materials (ICOTOM 15), June 1–6, 2008 Pittsburgh, Pennsylvania, USA, 2008, pp. 197–204.
[17] O.L. Garcia, R. Petrov, L. Kestens, Local characterization of void initiation on IF steel by FIB-EBSD technique in: A.D. Rollet (Ed.), Applications of Texture Analysis, Ceramic Transactions 201A, Collection of Papers Presented at the 15th International Conference on Texture in Materials (ICOTOM 15), June 1–6, 2008 Pittsburgh, Pennsylvania, USA, 2008, pp. 693–700.
[18] O. Melnikov, R. Tyshkevich, V. Yemelichev, V. Sarvanov, Lectures on Graph Theory, Nauka, Moscow, 1990.
[19] G.L. Dirichlet, Über die Reduktion der positiven quadratischen Formen mit drei unbestimmten ganzen Zahlen, Journal für die Reine und Angewandte Mathematik 40 (1850) 209–227.
[20] G. Voronoi, Nouvelles applications des paramtres continus la thorie des formes quadratiques, Journal fï die Reine und Angewandte Mathematik 133 (1907) 97–178.
[21] B. Barber, D.P. Dobkin, H. Huhdanpaa, The Quickhull algorithm for convex hulls, ACM Transactions on Mathematical Software 22 (1996) 469–483.
[22] B. Sander, Gefügekunde der Gesteine, Springer, Vienna, 1930.
[24] R. Hielscher, F. Bachmann, MTEX 3.2 – A Texture Calculation Toolbox, 〈http://mtex.googlecode.com〉, 2011.